Crystal Structure of Phospholipase A_2 Complex with the Hydrolysis Products of Platelet Activating Factor: Equilibrium Binding of Fatty Acid and Lysophospholipid-Ether at the Active Site May Be Mutually Exclusive[†,‡]

Ying H. Pan,[§] Bao-Zhu Yu,[§] Otto G. Berg,[||] Mahendra K. Jain,[§] and Brian J. Bahnson*[,§]

Department of Chemistry and Biochemistry, University of Delaware, Newark, Delaware 19716, and Department of Molecular Evolution, Uppsala University Evolutionary Biology Center, Uppsala, Sweden

Received September 30, 2002

ABSTRACT: We have solved the 1.55 Å crystal structure of the anion-assisted dimer of porcine pancreatic group IB phospholipase A2 (PLA2), complexed with the products of hydrolysis of the substrate platelet activating factor. The dimer contains five coplanar phosphate anions bound at the contact surface between the two PLA2 subunits. This structure parallels a previously reported anion-assisted dimer that mimics the tetrahedral intermediate of PLA2 bound to a substrate interface [Pan, Y. H., et al. (2001) *Biochemistry 40,* 609−617]. The dimer structure has a molecule of the product acetate bound in subunit A and the other product 1-octadecyl-*sn*-glycero-3-phosphocholine (LPC-ether) to subunit B. Therefore, this structure is of the two individual product binary complexes and not of a ternary complex with both products in one active site of PLA2. Protein crystals with bound products were only obtained by cocrystallization starting from the initial substrate. In contrast, an alternate crystal form was obtained when PLA2 was cocrystallized with LPC-ether and succinate, and this crystal form did not contain bound products. The product bound structure has acetate positioned in the catalytic site of subunit A such that one of its oxygen atoms is located 3.5 Å from the catalytic calcium. Likewise, a longer than typical Ca-to-Gly^{32} carbonyl distance of 3.4 Å results in a final Ca coordination that is four-coordinate and has distorted geometry. The other oxygen of acetate makes hydrogen bonds with $N_{\delta 1}$−His^{48}, $O_{\delta 1}$−Asp^{49}, and the catalytic assisting water (w7). In contrast, the glycerophosphocholine headgroup of LPC-ether in subunit B makes no contacts with calcium or with the catalytic residues His^{48} or Asp^{49}. The tail of the LPC-ether is located near the active site pocket with the last nine carbons of the *sn*-1- acyl chain refined in two alternate conformations. The remaining atoms of the LPC-ether product have been modeled into the solvent channel but have their occupancies set to zero in the refined model due to disorder. Together, the crystallographic and equilibrium binding results with the two products show that the simultaneous binding of both the products in a single active site is not favored.

Porcine pancreatic phospholipase A_2 (PLA2[1]), which catalyzes the hydrolysis of the *sn-2*-acyl substituent of glycerophospholipids, has served as a useful prototype for elucidating the mechanism for an enzyme that functions at a lipid-aqueous interface (*3*−*5*). The 14 kDa family of secreted phospholipase A_2 enzymes, are water-soluble enzymes that associate to an organized interface as a functionally active monomer to access their substrate and processively carry out the catalytic turnover (*3, 5*−*8*). PLA2 must make critical and specific interactions along a face of the protein that contacts this interface, called the i-face, to reach its fully activated form (*9*). Once associated to the membrane surface along the i-face, the enzyme binds substrate from the aggregated substrate interface. The resulting interface bound enzyme−substrate complex is influenced by specific anionic interactions of the interface to give an activated form (*6*), which undergoes esterolysis in the chemical step to form products.

In the search for functionally relevant structural information, the crystal structures of the anion-assisted dimer forms of PLA2 (*1*) and proPLA2 (*10*) with an active site directed *sn*-2-tetrahedral mimic have provided several key insights into the catalytically relevant features of the active form of PLA2 at the interface. For example, the structural differences seen in the catalytic site of the anion-assisted dimer of the PLA2 and its zymogen form suggest a basis for the impaired k^*_{cat} of proPLA2. As the mimic for the interface bound form

[†] The research was supported by NIH Grant GM-29703 to M.K.J. and B.J.B. and the Swedish Natural Science Research Council to O.G.B.

[‡] Coordinates for the structure of the phospholipase A_2 complexed with products acetate and 1-octadecyl-*sn*-glycero-3-phosphocholine have been deposited in the Protein Data Bank under code 1L8S.

* Corresponding author. B.J.B.: telephone, 302-831-0786; fax, 302-831-6335; e-mail, bahnson@udel.edu.

[§] University of Delaware.

[||] Uppsala University.

[1] Abbreviations: B-factor, temperature factor; i-face, interface binding surface of enzyme; deoxy-LPC, 1-hexadecyl-propanediol-3-phosphocholine; DHG, (*R*)-*2*-dodecanoyl-amino-1-hexanol-phosphoglycol; MG14, 1-O-octyl-2-heptylphosphonyl-sn-glycero-3-phosphoethanolamine; LPC-ether, 1-*O*-octadecyl-*sn*-glycero-3-phosphocholine; MA, myristic acid; MJ33, 1-hexadecyl-3-(trifluoroethyl)-*sn*-glycero-2-phosphomethanol; PAF, 1-*O*-octadecyl-2-acetyl-sn-glycero-3-phosphocholine, also called platelet-activating factor; PDB, Protein Data Bank; PLA2, 14 kDa phospholipase A_2 group IB from porcine pancreas; PLA2−products, anion-assisted dimer of PLA2 complexed with products acetate and LPC-ether; R_{free}, free *R*-factor; $R_{working}$, working *R*-factor; RMSD, root-mean-square deviation; 69-loop, residues 59−75 of PLA2.

10.1021/bi026922r CCC: $22.00
Published on Web 11/15/2002

Scheme 1: Hydrolysis Reaction of PAF

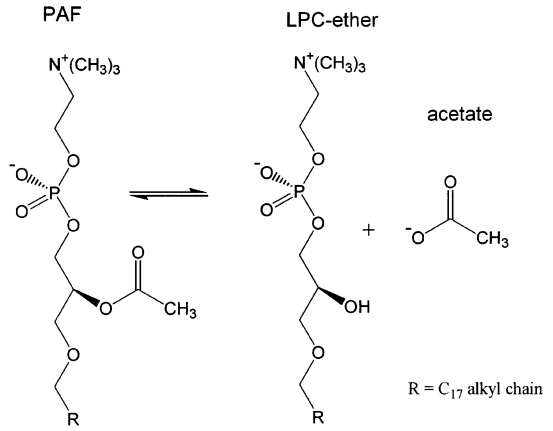

of the active enzyme, the anion-assisted dimer structures of PLA2 with 5-coplanar anions provided a model of the distinguishing feature to this interfacial binding. Here, the i-face of PLA2 contains a collar of anion binding sites that surround a hydrophobic patch through which the substrate accesses the catalytic residues during the turnover cycle.

Structures that mimic the interface-bound activated form of PLA2 allow investigations into discrete steps along the enzyme's mechanistic pathway. As mentioned above, a structure with an *sn-2*-tetrahedral mimic of the esterolysis reaction bound to an interface has already been reported (*1*). Another informative structural target would be an enzyme−substrate complex. However, determination of a high-resolution structure for an enzyme−substrate complex is complicated by an equilibrium constant of the PLA2 reaction that favors the product fatty acid and mono-alkyl phospholipid. Despite this thermodynamic preference, structural attempts have likewise failed to obtain an enzyme−product complex crystal structure for any PLA2 enzyme, indicating an as yet unknown complication to form ordered protein crystals of the product complex. Structures of the enzyme−product forms are essential elements in any attempts to map the active site events along the reaction coordinates and possibly the structural changes along the reaction trajectory. Furthermore, such information is deemed to be useful for understanding the regulatory mechanisms and for designing mechanism based inhibitors for potential therapeutic targets of inflammation to allergenic responses elicited in humans by 10 different genes for 14 kDa PLA2s (*3*).

Results in this paper extend the understanding of the product binding to PLA2 based on the crystal structure of the anion-assisted dimer form of porcine pancreatic PLA2 containing the products of hydrolysis of the PLA2 substrate platelet activating factor (PAF) in the active site (Scheme 1). The crystals of the product complex were formed by the cocrystallization of PLA2 with 3.9 mM of the substrate PAF. As expected on the basis of the known thermodynamics of the reaction and the observed rate of hydrolysis, PAF has been hydrolyzed to give the products, 1-*O*-octadecyl-*sn*-glycero-3-phosphocholine (LPC-ether) and acetate (*11*). Both these products are modeled in the reported crystal structure. Surprisingly, however, one of the subunits in the anion-assisted dimer crystal form contained only LPC-ether and the other subunit contained only the product acetate. Together with independent equilibrium binding studies at the phospholipid interface, these results show that the simultaneous binding of both the products in a single active site is not favored.

EXPERIMENTAL PROCEDURES

Crystallization of the PLA2 Product Complex and X-Ray Data Collection. Porcine pancreatic PLA2 was obtained as described before (*12*). A stock solution of the substrate 1-*O*-octadecyl-2-acetyl-sn-glycero-3-phosphocholine (PAF) from Avanti was prepared (21.4 mM) in deionized water. Protein crystals of the PLA2−product complex were grown at 25 °C, from 2.0 μL hanging drops containing 15 mg/mL PLA2, (1.1 mM enzyme), 10 mM $CaCl_2$, 3.9 mM PAF, 25% PEG 3500, 0.1 M Na^+-acetate, and 0.2 M NaH_2PO_4 buffer at pH 4.6. Crystals initially appeared in 2 days and ultimately grew to the dimensions 0.5 × 0.5 × 0.1 mm after 7 days. Under the same crystallization condition, but without the substrate PAF added, only protein aggregates were obtained. Furthermore, when the crystallization was performed with the same crystallization condition, but with 1-*O*-octadecyl-*sn*-glycero-3-phosphocholine (LPC-ether) and succinate, an alternate crystal form was obtained. An X-ray diffraction data set was collected from a single crystal on a Rigaku-RU300 rotating anode generator with a RAXIS IV image plate area detector. The crystals were preequilibrated in a cryo-protecting and stabilizing solution made of the crystallization condition reported above with the addition of xylitol (25% saturating) as the cryo-protectant and then flash frozen in the −180 °C nitrogen cryo-stream. The Programs DENZO and SCALEPAK (*13*) were used for data processing and scaling. The PLA2−product complex crystal belongs to space group $P3_1$ with two molecules of PLA2 in the asymmetric unit.

Molecular Replacement. The crystal structure of the PLA2 product complex was solved by molecular replacement using the program AMORE (*14*) from the CCP4 package (*15*). Protein coordinates of one dimer subunit from a previously refined PLA2−inhibitor complex (PDB code: 1FXF) was used as the search model. The final molecular replacement solution included two subunits of PLA2 in the asymmetric unit with an *R*-value of 32.7% and a correlation factor of 62.9%.

Crystallographic Refinement. The crystals of the PLA2−product complex have symmetry of the space group $P3_1$. The crystallographic refinement was initially complicated by mehrohedral twinning (*16*). The refinement of the product complex is in an isomorphous space group and unit cell as a previously reported anion-assisted dimer structure of PLA2 that displayed mehrohedral twinning as well (*1*). The approach and programs used to correct the twinning during the refinement and resulting electron denisity maps has been discussed extensively (*1*) and will be summarized below. Initial refinement was carried out using the program CNS (*17*) without the use of a twin correction. The purpose was to use certain features of the CNS refinement routine, such as simulated annealing refinement, to ensure that the structure was not trapped in an incorrect local minimum. Initial rounds of refinement were performed using the CNS program that applied standard procedures, such as rigid body, positional, simulated annealing, and individual temperature factor (*B*-factor) refinement. Iterative model improvement was achieved using the graphics programs CHAIN (*18*) or O (*19*), followed by further rounds of CNS refinement. This process converged and brought the free *R*-value (R_{free}) to a value of 0.332 and the working *R*-value ($R_{working}$) to a value of 0.252 using X-ray

diffraction data to a resolution of 2.2 Å. The difference Fourier electron density map ($F_o - F_c$) contoured at 3σ showed identifiable density for parts of the products in both the subunits. Five phosphate ions, two calcium ions, and 239 water molecules were added to the model. A single round of refinement to a resolution to 1.8 Å brought the R_{free} to 0.293 and $R_{working}$ to 0.232. Attempts using a twin correction in the program CNS were unsuccessful to improve the model. Likewise, the difference electron density maps obtained from CNS refinement with a twin correction was not of sufficient quality to unambiguously model the bound products into subunit A or B.

In the final stage, the refinement was switched to the program SHELX-97 in order to incorporate a twin correction to the refinement routine (*16*). The twinning is merohedral, where the two twin components of the reciprocal lattices coincide exactly. In the refinement using shelxl-97, the twin law $\mathbf{R} = [0\ 1\ 0\ 1\ 0\ 0\ 0\ 0\ -1]$ was applied, where **R** is the matrix that transforms the *hkl* indices of one component into the other. The twin fraction was consistently found to be greater than 0.45 along A and B and negligible along C by the online twinning test of Yeates [ref *16* and URL:http://www.doe-mbi.ucla.edu/Services/Twinning/]. Following SHELX-97 refinement using a twin correction, the electron density difference map at 1.8 Å ($2F_o - F_c$) was used to build the product models with clearly identifiable densities for acetate in subunit A and for the two calcium, five phosphate ions, and 281 solvent molecules. Subunit B showed $F_o - F_c$ difference electron density consistent with a portion of the LPC-ether product. Several possible orientations of the LPC-ether molecule were modeled into the structure with all but one failing to satisfy the data and at the same time be chemically reasonable. At this point, the single unambiguous orientation of LPC-ether included nine carbons of the sn-1 alkyl tail. Further inspection of $F_o - F_c$ difference electron density maps did not support any portion of the remainder of the LPC-ether molecule bound in an ordered fashion. However, difference maps supported two alternate conformations of the alkyl tail. The final model reported has the terminal nine carbons of the *sn*-1 acyl chain refined in two alternate conformations. The remainder of the LPC-ether molecule has been positioned to avoid bad contacts. The corrected model was then subjected to a final cycle of least squares refinement in SHELX-97 with twin correction routines implemented. The twin fraction refined to 0.49958 after 10 cycles of conjugated gradient least-square refinement. The final model was refined to a value for R_{free} of 0.249 and $R_{working}$ of 0.184.

Fluorescence Emission Spectroscopy. The change in fluorescence emission (with excitation at 280 nm) was monitored on a SLM-Aminco AB2 Luminescence Spectrometer with magnetic stirring in a cuvette containing 1.5 mL of 100 mM NaCl, 1 mM $CaCl_2$, and 10 mM pH 8.0 Tris (*20*). The most significant changes in fluorescence are due to a varied environment of the sole Tyr^3 of PLA2. Difference spectra were performed with a concentration of 3.3 μM PLA2. Typically, the slit widths were kept at 4 nm each, and the sensitivity was adjusted to 1% for the Raman peak corresponding to the same excitation wavelength from the buffer blank. The relative change in fluorescence, δF, is defined as $(F - F_o)/F_o$, where F_o and F are the intensity initially and following the indicated additive, respectively.

Table 1: PLA2−Products Complex X-Ray Data Collection and Refinement

Crystal Data	
space group	$P3_1$
cell parameters	
$a = b$ (Å)	65.2
c (Å)	63.0
subunits/asymmetric unit	2
X-Ray Data	
total reflections	266,326
unique reflections	43,050
resolution limit (Å)	1.55
completeness (%)	99.0 (95.9)[a]
R_{merge}[b]	6.2 (36)[a]
Refinement	
resolution range (Å)	8.0−1.55
$R_{working}$[c]	0.184
R_{free}[c]	0.249
RMSD observed	
bond lengths (Å)	0.010
angles distance (Å)	0.028
total water molecules	312

[a] The number is parentheses is for the highest resolution shell of data from 1.55−1.61 Å. [b] $R_{merge} = \Sigma|I_o - I_a|/\Sigma I_a$, where I_o is the observed intensity and I_a is the average intensity, the sums being taken over all symmetry related reflections. [c] R-factor $= \Sigma||F_o| - |F_c||/\Sigma|F_o|$, where F_o is the observed amplitude and F_c is the calculated amplitude. R_{free} is the equivalent of $R_{working}$, except that it is calculated for a randomly chosen set of reflections that were omitted (10%) from the refinement process (*17*).

Dissociation Constants for the PLA2 Complexes by the His[48] Protection Method. Detailed experimental protocols for the determination of equilibrium dissociation constants by the protection method have been described previously (*21*, *22*). A theoretical basis for the analysis relevant for the binding of one or both products simultaneously is developed in an Appendix. Equilibrium dissociation constants for the active site directed ligands, such as the product (K_P*) bound to PLA2, was determined in 1 mM NaCl at pH 7.4 in 100 mM NaCl and 50 mM cacodylate buffer at pH 7.3 and 23 °C. Values of the interfacial equilibrium parameters are expressed in mole fraction units and the estimated uncertainty in the dissociation constant values is less than 30%.

RESULTS

We present the first structure of a secreted PLA2 in complex with products of the esterolysis reaction. The data collection and refinement statistics of the 1.55 Å structure of the phosphate-assisted dimer form of the PLA2−product complex are summarized in Table 1. To our surprise, the crystal structure contained the two products of hydrolysis of the substrate PAF, but each bound to separate subunits with active sites in a similar conformation (Figure 1). The quality of the structure can be assessed from the electron densities for the acetate and LPC-ether bound product molecules that are shown in panels C and D, respectively, of Figure 1. Each subunit contains a catalytic calcium. However, the acetate product is coordinated in the active site of one subunit and the sn-1 alkyl tail of the LPC-ether product is bound in the hydrophobic substrate slot of the second active site. On the basis of the arguments developed below, the structure is suggestive that the acetate and LPC-ether product molecules were initially derived from a single molecule of the substrate PAF.

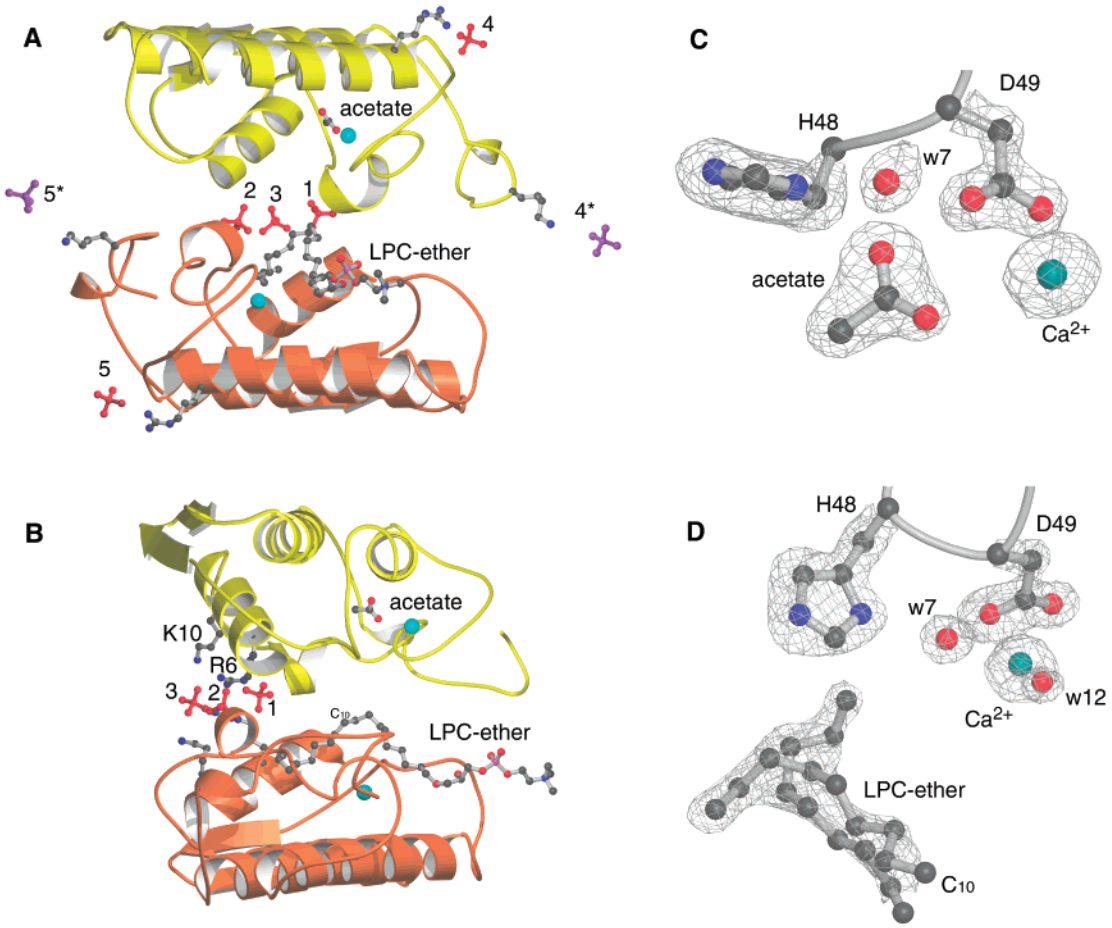

FIGURE 1: Structure of the anion-assisted dimer of PLA2 with bound reaction products acetate and LPC-ether. (A) The two subunits of the protein dimer are represented by a ribbon diagram with subunit A (top) in yellow and subunit B (bottom) in orange. Subunit A has bound acetate, and subunit B has bound LPC-ether product. The phosphate anions (red) of one asymmetric unit are numbered 1−5. Phosphate anions 4* and 5* (purple) are crystallographically identical to 4 and 5, respectively, and are included in this figure to demonstrate the coplanar nature of five phosphate anions 1−3, 4*, and 5*. (B) The two subunits of the product complex are shown from a side view from panel A. The Arg^{6} and Lys^{10} side chains from subunits A and B (labeled from subunit A) are shown coordinating with phosphates 1−3. Each view demonstrates a possible orientation of the portion of the LPC-ether molecule that was not observed by the crystallographic data. The final 9-carbons of the C_{18} chain (carbons 10−18) of the LPC-ether were refined with the X-ray data. The position of the 10th carbon (C_{10}) of the C_{18} alkyl chain is labeled. (C) PLA2−products structure $2F_o - F_c$ electron density difference maps contoured at 1.8 σ, including the bound reaction products of acetate in subunit A and (D) the final 9-carbons of the C_{18} alkyl tail of the LPC-ether in subunit B contoured at 1.8 σ. The bound products are shown in reference to the active site Ca, His^{48}, Asp^{49}, and water w7, which is referred to as the assisting water (formerly[2] referred to as w6). The LPC-ether bound active site has the axial water w12 coordinated to calcium. The figure was made using the programs MOLSCRIPT (*33*), POVSCRIPT (http://people.brandeis.edu/~fenn/povscript/), and POVRAY http://www.povray.org).

Anion-Assisted Dimer of PLA2. Overall, the backbone structure of the anion-assisted dimer of PLA2 complexed with the products acetate and LPC-ether (PLA2−products) is quite similar to PLA2 structures previously reported (*23*−*25*). Five coplanar phosphate ions were found at the intersubunit contact surface, as shown in Figure 1A,B. A particularly important comparison can be made to the previously reported anion-assisted dimer of PLA2 complexed with the active site directed sn-2-tetrahedral mimic 1-hexadecyl-3-(trifluoroethyl)-*sn*-glycero-2-phosphomethanol (MJ33) (*1*). This previously reported structure had been suggested to be a mimic of the tetrahedral intermediate of the enzyme when it is bound to an interface. The overlay of subunit A from the PLA2−products complex and PLA2−MJ33 structures has an overall and main-chain root-mean-squared deviation (RMSD) of 0.73 and 0.31 Å, respectively. Similarly, the overall and main-chain RMSD between subunit B in the two dimer structures are 0.91 and 0.48 Å, respectively. These differences are similar to those observed from a comparison of the two subunits of the PLA2−products structure, which has an overall and main-chain RMSD of 0.96 and 0.41 Å, respectively. The orientation of subunit A to subunit B is likewise very similar to the PLA2−MJ33 structure previously reported. For example, one way to evaluate this relationship is to define the angle between the two vectors connecting the N- and C-terminus of each of the two subunits. This analysis yields an angle of 117.74° and 117.70° for the product and MJ33 structures, respectively. Likewise, the positions of the five-coplanar phosphate anions are virtually identical to the positions of phosphate anions (PDB code: 1FXF) in the previously reported PLA2−MJ33 complex (*1*). As a result of these similarities, the contact surface in the PLA2−product dimer, which is

[2] The assisting water of the Ca-coordinated oxyanion mechanism had been previously (*1*, *2*) referred to as w6. However, the position of the assisting water in the present structure and the previous interface mimic structure (*1*) aligns with water w7 from the ligand free PLA2 active site waters (*3*).

Table 2: RMSD Comparison of Interfacial Residues in the Anion-Assisted PLA2−Acetate Complex with Other Group IB PLA2s

porcine acetate (1L8S)[a]	porcine MJ33 (1FXF)	porcine DHG (5P2P)	bovine no ligand (1UNE)	bovine MG14 (1MKV)	bovine MJ33 (1FDK)
Leu[2]	0.17[b]	1.15	0.69	0.15	0.25
	1.87[b]	**2.81**	**2.28**	**1.85**	**1.50**
Trp[3]	0.17		0.57	0.49	0.60
	0.26	[c]	1.38	**6.92**	**5.88**
Arg[6]	0.20	0.95			
	0.33	**2.18**	[c]	[c]	[c]
Leu[19]	0.15	0.67	1.18	**1.45**	**1.61**
	1.83	0.98	1.29	**1.83**	1.39
Met[20]	0.09	0.65			
	1.13	**3.68**	[c]	[c]	[c]
Asn[23]	0.24	0.26	0.44	0.56	0.69
	0.73	0.46	**1.65**	0.83	**1.91**
Asn[24]	0.22	0.58	0.44	0.66	0.91
	1.70	**3.03**	**2.54**	**1.85**	**2.51**
Leu[31]	0.48		0.59	1.08	1.14
	2.27	[c]	**2.21**	**2.07**	**2.14**
Val[65]	1.05		**4.45**	**4.40**	**4.21**
	1.34	[d]	**3.70**	**5.79**	**5.71**
Asp[66]	0.62		**4.64**	**3.93**	**3.45**
	2.44	[d]	**8.85**	**6.05**	**6.15**
Asn[67]	0.35		**3.09**	**2.36**	**1.94**
	1.37	[d]	**3.76**	**3.06**	**1.97**
Tyr[69]	0.35	1.14	1.06	0.97	0.92
	0.53	**4.99**	**4.38**	**4.08**	**2.18**
Thr[70]	0.33	0.73	0.66	1.28	1.09
	0.31	1.24	1.27	**2.07**	**2.73**
Ser[72]	0.35	0.58			
	0.32	0.64	[c]	[c]	[c]
Asn[117]	0.15	0.69	0.83	1.27	1.73
	0.30	**2.44**	**2.13**	**2.81**	**2.95**
Leu[118]	0.52	1.04	1.01	1.16	1.40
	0.55	0.99	**2.25**	**2.26**	**2.43**
Asp[119]	0.49	1.25	0.87	0.74	0.71
	1.63	0.92	**1.45**	**2.29**	1.01
Thr[120]	0.35	1.21	**2.68**[e]	**2.66**	**3.04**
	0.29	1.43	**5.22**	**4.81**	**4.92**
Lys[121]	0.35	1.24	**1.61**	1.43	**1.52**
	0.97	**3.20**	**2.05**	**3.84**	**4.25**

[a] Subunit A of PLA2−products complex with the product acetate bound. The source, active site ligand and PDB code (in parentheses) is listed for each structure that is compared. [b] Numbers in the first and second rows are main-chain and side-chain RMSDs, respectively. RMSD greater than 1.5 Å is shown in bold. [c] The residue is different from that of porcine PLA2 due to mutation or deletion; hence, the RMSD is not available. [d] Residues 62−67 were deleted from the protein sequence. [e] The large RMSD is due to the mismatches in a.a. sequence between bovine and porcine PLA2s at the C-terminus.

postulated to correspond to the i-face, is virtually identical to that seen in the anion-assisted dimer of PLA2 complexed with MJ33.

These comparisons indicate that the backbone orientation, the coordination for the five-anion binding sites, the side chains at contact surface between the subunits, and the relative orientation between the two subunits in the PLA2−products and PLA2−MJ33 structures are virtually identical. Comparison of the PLA2−products structure to other PLA2 structures with bound ligands reveals some notable differences in the interface-binding region of PLA2, as shown in Tables 2 for the PLA2·acetate complex of subunit A. The second column of Table 2 corresponds to a structural form of PLA2 that mimics the enzyme bound to an interface (*1*). The last four columns of Tables 2 are structures of PLA2 that mimic the enzyme structure in an aqueous noninterfacial state. The most notable differences shown for this latter group of structures are in a region called the 69-loop (residues 59−75 of PLA2) that are a critical interfacial binding loop that contains Tyr[69]. Additional differences that are observed in the interfacial binding region may likewise be essential to the ultimate regulation of PLA2 activity bound to an interface. Overall, the position of interfacial side chains in the anion-assisted PLA2−acetate product complex is very similar to the anion-assisted dimer structure with MJ33 bound. In contrast, other structures of PLA2 that do not mimic an interface bound form have significant structural differences in the interfacial region.

Binding Sites for the Two Products. The locations of the acetate in subunit A and LPC-ether alkyl tail in subunit B of the anion-assisted dimer was modeled from the interpretation of $2F_o - F_c$ and $F_o - F_c$ electron density difference maps (Figure 1C,D). The average B-factor for both the product acetate in subunit A and the final 9 carbons of the sn-1 alkyl tail (C_{10}−C_{18}) of LPC-ether in subunit B was about 30 Å^2, consistent with the bulk of the protein. The remainder of the LPC-ether product had atomic occupancies set to zero and these atoms were not refined in the final rounds of refinement due to disorder. However, the positioning of the remainder of the LPC-ether has been modeled and is depicted in Figure 1A,B.

In subunit A, the acetate product binds tightly at the catalytic site as shown in Figure 2. One of the acetate oxygens is located 3.5 Å from the catalytic Ca. This distance is significantly longer than a typical Ca−oxygen ligand distance of 2.3−2.6 Å. This oxygen is hydrogen bonded to a water, labeled w13 in Figure 2A, that has not been seen in previous PLA2 structures. The other acetate oxygen is located at a position that is frequently occupied with the "second shell" water w6 seen in several other PLA2 structures (*25*, *26*). This same acetate oxygen is hydrogen bonded to His[48]. This acetate oxygen displays close contacts with several other atoms of the active site, which are summarized in Table 3. One notable interaction is with water w7. This water is also in the second coordination shell of calcium and is referred to as the assisting water[2] in the oxyanion mechanism (*1*). The absence of this water represents an inactive form of PLA2 (*10*); the water w7 has only been observed in PLA2−ligand structures that mimic an activated form of the enzyme (*1*), as in the structure reported here. The assisting water w7 also has a hydrogen bonding interaction to Try[69]. The position of the 69-loop and the presence or absence of the Tyr[69] interaction to active site waters and ligands have been suggested to be a determinant of enzyme activity (*10*).

A comparison of the calcium binding loops of the acetate bound subunit A and a ligand-free structure of PLA2 (*25*) is shown in Figure 2B. The alignment reveals that the main chain conformations are very similar, with the exception occurring at position Gly[32]. The difference observed for Gly[32] relative to other PLA2 structures is most pronounced in the acetate bound subunit A where calcium is four-coordinate. Here Gly[32] has an unusual dihedral angle. As a result, the Ca to oxygen distance for the carbonyl oxygen of Gly[32] is 3.4 Å, much longer than the expected Ca−ligand distance of 2.4 Å. Additionally, the Ca position is shifted away from the substrate binding pocket, resulting in a Ca-to-acetate oxygen distance of 3.5 Å. An additional significant difference

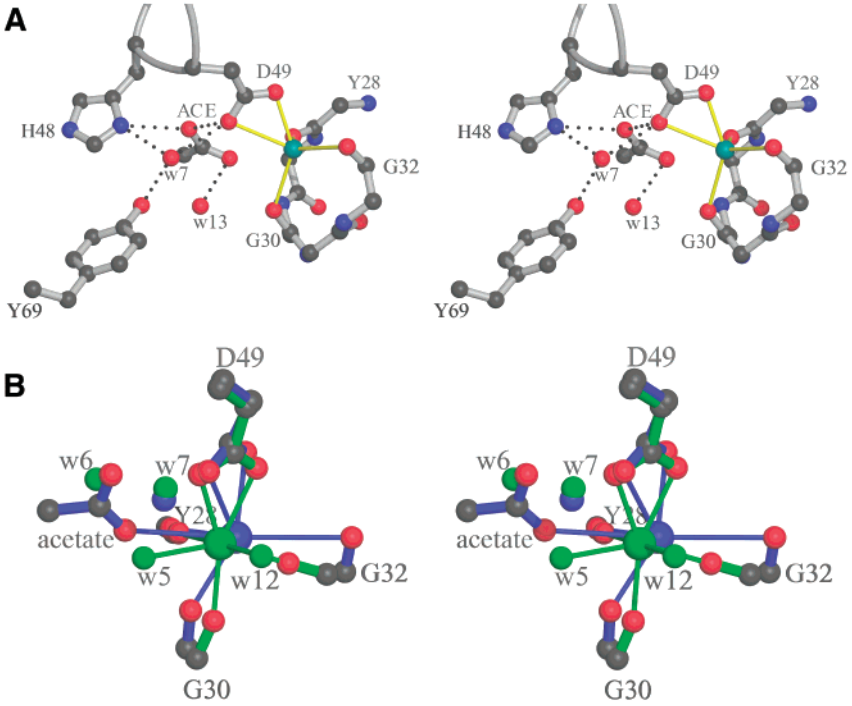

FIGURE 2: Stereoview of the coordination of the acetate product with calcium and PLA2. (A) The calcium (green) does not have significant interactions with the carbonyl oxygen of the product acetate and the backbone of Gly^{32}. The calcium interactions are shown as a solid yellow bonds. Hydrogen bonding distances less than 3.2 Å are shown as dashed black lines. A more complete description of inter atomic bond distances is shown in Table 3. (B) Overlay of the PLA2−acetate complex shown in blue with the structure of PLA2 without a bound ligand (*25*) shown in green. The positions of the two oxygens of acetate are roughly superimposed over the positions of waters w5 and w6 from the ligand free structure. Each structure has a water molecule at position w7, which is referred to as the assisting water. The position of the Ca in the acetate complex is shifted relative to the ligand free enzyme. Most notably, the position of the Ca loop at position Gly^{32} is changed to accommodate the new Ca position. The figure was made using the programs MOLSCRIPT (*33*), POVSCRIPT (http://people.brandeis.edu/~fenn/povscript/), and POVRAY (http://www.povray.org).

Table 3: PLA2 Active Site Distances in the A-Subunit with Complexed Acetate

atom 1	atom 2	distance (Å)
w7[a]	acetate O22	2.80
Asp^{49} OD1	acetate O22	2.85
His^{48} ND1	acetate O22	2.89
Cys^{45} O	acetate O22	3.03
Tyr^{28} O	acetate O2H	2.83
w181	acetate O2H	3.01
Gly^{30} O	acetate O2H	3.07
Gly^{30} N	acetate O2H	3.21
Ca^{2+}	acetate O2H	3.50
Tyr^{69} OH	w7	2.76
Tyr^{69} OH	w13	2.43
His^{48} ND1	w7	2.99
Asp^{49} OD1	w7	2.75
Asp^{49} OD1	Ca^{2+}	2.93
Asp^{49} OD2	Ca^{2+}	2.50
Tyr^{28} O	Ca^{2+}	2.69
Gly^{30} O	Ca^{2+}	2.85
Gly^{32} O	Ca^{2+}	3.36

[a] Water 7, designated w7, is in an equivalent position to the assisting water of the anion-assisted dimer structure of PLA2 complexed with MJ33 (*1*).

is the absence of an axial ligand at the position of w12 in the ligand free structure. Together, these differences in the acetate bound form of subunit A define the Ca as four-coordinate with distorted geometry.

In contrast to subunit A, the sn-1 alkyl tail of the LPC-ether product is coordinated into subunit B. Attempts were made at modeling partial occupancies of additional atoms beyond the ninth carbon from the end of the *sn*-1 tail. However, these attempts led to inferior electron density maps. The final model of the last nine carbons (C_{10}−C_{18}) of the LPC-ether has been refined with two alternate conformations as shown in Figure 1D. The occupancy of these two conformations was refined to 48% and 52%. For the remainder of the LPC-ether product, the occupancies of each of the atoms were set to zero, but included in the refined model. This provides a possible orientation for the disordered portion of the molecule relative to the two subunits. The entire LPC-ether molecule is depicted in Figure 1A and from a side view in Figure 1B, with the understanding that the X-ray data were used to accurately position only the nine terminal carbons of the sn-1 alkyl chain. Adjacent to the alkyl tail in the active site slot of subunit B, the seven-coordinating ligands for calcium are the same as those seen with the native PLA2 with an unoccupied active site (*23*, *25*). Notably, the calcium coordination in subunit B retains the axial water (w12) and also one of the other active site waters in the second coordination shell (w7) (*10*).

The 69-Loop. The stretch of residues from 59 to 75 that includes Tyr^{69} (69-loop) in both subunits-A and -B of the PLA2−product structure is ordered and almost identical (Table 2) to that reported in the anion-assisted PLA2−MJ33 complex structure (*1*). A comparison of each of the subunits of the PLA2−products structure with the PLA2−MJ33 structure has a main chain RMSD of 1.0 Å for residues 61−69. These results suggest that irrespective of the nature of the mimic in the active site, the 69-loop of PLA2 assumes a definite conformation in contact with an interface. As

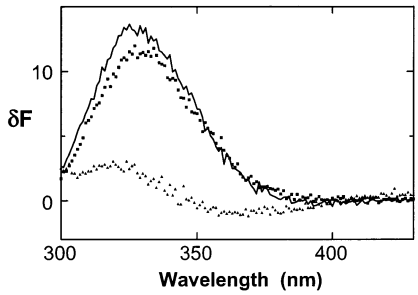

FIGURE 3: The myristate induced change in the fluorescence emission spectrum of PLA2 equilibrated under the following conditions. In each case, myristate was added to the vesicle interface to a concentration of a 0.1 mol fraction. Top solid line, to 1.05 mM deoxy-LPC; middle dotted line, to 0.2 mol fraction LPC-ether in 1.05 mM deoxy-LPC; or bottom dotted line, to 1.05 mM LPC-ether alone. An independent control showed that the addition of the same amount of myristate to PLA2 in the absence of an interface had no noticeable change in the emission spectrum.

Scheme 2: PLA2 Equilibrium Binding of Fatty Acid (FA) or LPC-Ether Products to the Interfacially Bound Form (E*)

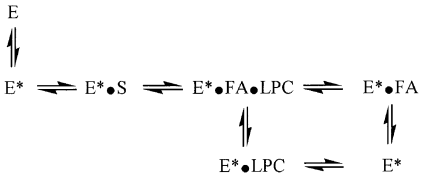

shown before, the 69-loop adopts alternate conformations in forms of PLA2 that represent inactive or less active forms of the enzyme (*10*).

Spectroscopic Evidence for the Occupancy of the Active Site. Independent evidence for the binding of LPC-ether or fatty acid to the active site of PLA2 bound to an interface was probed by fluorescence emission spectroscopy. Here, the active site-directed ligand binding was monitored indirectly by following fluorescence changes imposed by the binding of the enzyme to the interface (E to E*). The binding of an active site directed ligand, such as the product acetate or LPC-ether, imposes a shift of the apparent equilibrium from E toward E* and E*P, as depicted in Scheme 2. The fluorescence emission characteristics of Trp^3 are significantly perturbed on the binding of the enzyme to the interface (*20*, *27*). A particularly instructive set of results is summarized in Figure 3, where the addition of myristate to a mixture of E and E* exhibits a significantly different effect on the enzyme bound to the interface. Here, the neutral diluent 1-hexadecyl-propanediol-3-phosphocholine (deoxy-LPC) provides an interface for PLA2 binding and does not occupy the active site. Therefore, addition of myristate or LPC-ether (results not shown) to the enzyme bound to deoxy-LPC-ether induces a large change in the Trp^3 emission. On the basis of the known values of K_d (1.6 mM for the deoxy-LPC interface), this increase is best interpreted as a myristate-induced shift from free PLA2 (E) to PLA2 bound to an interface (E* + E*−fatty acid) as shown in Scheme 2. In the bound forms of the enzyme, Trp^3 becomes more shielded from water and therefore results in an increase in fluorescence. The mole-fraction-dependent binding of either myristate or LPC-ether at the interface will shift all of the PLA2 into the interface bound forms. Controls showed that the effects induced by myristate or by LPC-ether require the presence of calcium and also require that the enzyme be bound to the interface. As expected, the deoxy-LPC induced change in the emission spectrum is not significantly affected by calcium. These results clearly show that myristate and LPC-ether preferentially bind to the E* form, and if there is any binding to the free E form, it occurs without a change in the Trp^3 fluorescence. However, these results cannot distinguish between the equilibrium binding of either a binary complex of PLA2·myristate or PLA2·LPC-ether or a ternary complex of PLA2·myristate·LPC-ether.

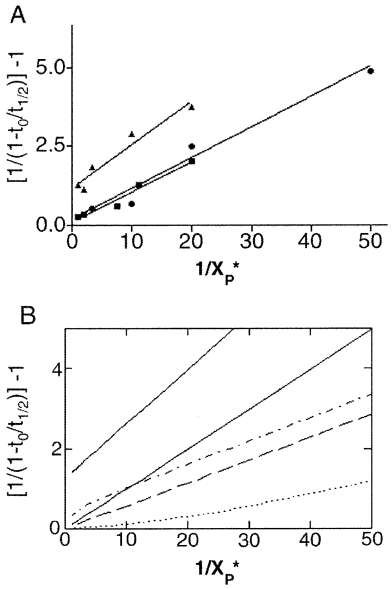

FIGURE 4: (A) The experimental relationship between the inactivation time for the E* form of PLA2 by *p*-bromophenacyl bromide without (t_o) or with an active site directed ligand ($t_{1/2}$) as a function of the reciprocal of the mole fraction ($1/X_p$*) of LPC-ether (triangles), myristic acid (filled circles), or LPC-ether + myristate at a ration of 1/1 (squares). The diluent in all three cases was 3.6 mM deoxy-LPC. (B) Calculated Scrutton-Utter plots for the conditions comparable to those for the experimental data shown in panel 7A and theoretically developed in the Appendix. The upper solid line is the best fit to the data for LPC-ether alone, giving K_1* = 0.06. The lower solid line is the best fit for myristate alone, giving K_2* = 0.10. The dashed curve is the expected result from eq 10 from Appendix when both products are present in equimolar amounts in the reaction mixture, and if binding of the two ligands is independent ($w = 1$), the dash−dot curve is for anticooperative binding ($w = 0.1$), and the dotted curve is for cooperative binding ($w = 10$).

The effect of myristate or LPC-ether added to the E*Ca form of the enzyme on the deoxy-LPC interface depends on the mole fraction of these active site directed ligands. From these titration curves, the mole fraction of the product at which half of the maximum change is observed has been calculated. Using a value of $K_d = 1.6$ mM (*28*), the corrected K_P* for myristate is about 0.04 mol fraction, and it is 0.06 mol fraction for LPC, with about 30% uncertainty in each value. These values are comparable to those obtained by the complementary His^{48} protection method.

His^{48} Protection Assay Supports Single Product Binding. An independent description of product binding to PLA2 is offered by an active site protection assay shown in Figure 4A. Ligand binding is monitored by the quantification of the alkylation protection to His^{48} if the active site is occupied with an active site directed ligand (*21*). Results in Figure 4A show that the occupancy of the active site changes linearly in each case, with the mole fraction of both the

products added in a 1:1 ratio. These results are consistent with the earlier results (*21*) with either one or both the products of hydrolysis of 1,2-dimyristoyl-phosphatidylcholine, except for the fact that no significant protection is observed with *sn-1*-myristoyl-phosphatidylcholine alone. A modest difference in the protection ability of the *sn-1*-ether and the *sn-1*-ester analogue of the lysophospholipid product suggests that the *sn-1*-ester group lowers the apparent affinity for the active site.

The linear dependence on X_P* in the presence of both the products is a surprising result. If both the products simultaneously occupied the active site and each contributed to the protection, the X_P* dependence would be a higher-order term. This is because the probability of simultaneous occupancy of the active site by both the products would increase at a higher mole fraction. The expected higher order dependence is demonstrated theoretically in Figure 4B, with a more detailed description given in the accompanying Appendix. This curvature is not seen with equimolar mixtures of the products of hydrolysis of dimyristoyl-phosphatidylcholine (Figure 4A) or with the products of hydrolysis of dimyristoyl-phosphatidylmethanol (*4*, *21*). As shown in Figure 4A, in the presence of myristate, the *y*-intercept is <0.02, i.e., the occupancy of the active site offers $>98\%$ protection against alkylation. In contrast, the *y*-intercept in the presence of LPC-ether is 0.5. Here 50% protection is offered by the binding of LPC-ether to the E* form of PLA2 at the interface. The K_P* values, calculated from the slopes of these lines, are 0.1 mol fraction for myristate and 0.06 mol fraction for LPC-ether.

The experimental results in the presence of equimolar LPC-ether and myristate, as well as for the equimolar mixture of lyso-phosphatidylmethanol and myristate [results not shown here, see refs *4* and *21*], suggest that the *y*-intercept is close to zero. Uncertainty in the extrapolated *y*-intercept results does not permit unequivocal resolution of all binding parameters. Using the single-ligand results ($K_1^* = 0.06$, $K_2^* = 0.1$, and $k_1/k_0 = 0.55$), eq 10 in the Appendix can be used to predict the protection when both products are present in the solution in equimolar amounts. If single-ligand binding remains the same, the only free parameter in this equation is the cooperativity factor *w* (eq 7). The expected results for some values of *w* have been plotted in Figure 4B. The expected result when both products are present cannot be fitted to the observed results (Figure 4A) with any choice of *w*. This shows that the presence of both products in the interface can also change the properties of the binding of single ligands. The case when both products are present in the interface is nearly superimposable to that for myristate alone (Figure 4A). The simplest suggestion is that the presence of myristate in the interface reduces the affinity of LPC-ether to the active site so that it does not compete with the binding of myristate. Such a possibility would be consistent with the results that suggest that LPC and myristate form a complex in the bilayer interface (*29*, *30*). It is possible to come close to the observed result also if K_2^* is increased to 0.3 (with $w = 1$), while the other parameters (K_1^* and k_1/k_0) remain the same. However, it will be possible to get good fits also for other combinations if all three binding parameters (K_1^*, K_2^* and *w*) and when the protection parameter k_1/k_0 are allowed to vary. Unfortunately, the experimental results do not permit the resolution of these and other possibilities.

DISCUSSION

Formation of the ternary complex E*·FA·LPC with both the products of hydrolysis in the active site of PLA2 is an obligatory step in the catalytic turnover cycle (Scheme 2). However, a key distinction of the PLA2−products structure is that the fatty acid product acetate or the product LPC-ether bind separately in the two subunits of the anion-assisted dimer, and roughly the same region of the active site pocket is occupied in both the binary complexes. On the basis of this observation, it is our assertion that each of these binary complexes is thermodynamically lower in energy than the ternary product complex. Acetate in subunit A reveals the mechanistically significant interactions of a sn-2 fatty acid product complex. In contrast, the alkyl tail of the LPC-ether is bound in the active site slot of subunit B. One should note that the structure reported here represents the binary complex product structure in an equilibrium sense and is not a kinetically trapped intermediate.

Although the structure is not directly representative of how the monomer behaves on a substrate interface surface, the structural model offers a framework to interpret the equilibrium binding results of PLA2 with bound sn-2 fatty acids and LPC-ether products. The equilibrium binding results corroborate the conclusion that the affinity of fatty acid or LPC-ether in the binary complexes is comparable. There is no evidence for the formation of the ternary complex under the His^{48} protection conditions, and the fluorescence emission changes are consistent with a model that LPC-ether and myristate compete for the same binding region. These results are interpreted below to suggest that the binary complexes are significantly different than the ternary complex that would result after the chemical step of the turnover cycle.

In relationship to the catalytic mechanism, the information from the acetate bound structure is mechanistically significant and represents the first structural information of products bound to PLA2. Acetate at a concentration of 100 mM is a component of the crystallization condition. The acetate observed in the crystal structure is likely in equilibrium with the bulk acetate and not solely derived as a direct product of substrate PAF hydrolysis. However, it is noteworthy that crystallization of PLA2 under analogous conditions, but with the LPC-ether and acetate in the buffer, failed to yield crystals. When acetate was replaced by succinate, an alternate crystal form was obtained with a structure that had no products bound in the active site. In contrast, the anion-assisted dimer form of PLA2 with bound acetate represents an active form of the enzyme.

It is significant that protein crystals in the anion-assisted dimer crystal form could only be obtained starting with the substrate PAF. It is reasonable to suggest that a single molecule of the substrate PAF is a required element to allow the anion-assisted dimer to form. The PLA2 catalyzed hydrolysis of PAF is likewise predicted to be slow under the conditions of protein crystallization. The rate of PAF hydrolysis is expected to be at least 3 orders of magnitude slower at pH 4.6 in the crystallization solution than that at pH 8.0, where PLA2 hydrolysis of PAF has been shown to have a turnover number of 3 s^{-1} (*11*). A bridging substrate PAF ligand is analogous to the inhibitor MJ33 that bridges

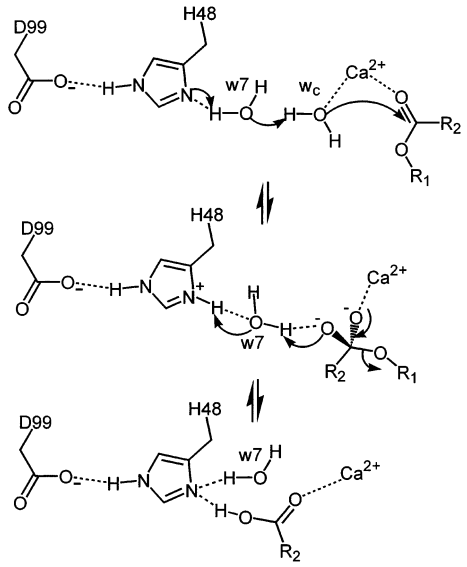

FIGURE 5: The water-assisted calcium-coordinate oxyanion mechanism of PLA2. The enzyme−substrate complex is depicted with a Ca-coordinated ester substrate and the catalytic water w_c. The catalytic water is bridged to His^{48} by the assisting water labeled w7. The tetrahedral intermediate is Ca-coordinated and bridged to His^{48} by the assisting water w7. The sn-2 product fatty acid is shown as a binary product complex. Notably, this complex has interactions to His^{48} from both the product fatty acid and the assisting water w7.

the two subunits of the previously reported anion-assisted dimer of PLA2 (*1*). The PAF and phosphate-anion-mediated dimerization can be thought of as a nucleation event that is happening throughout the crystal growth phase. An initial monomer of PLA2 complexed with PAF then associates with phosphate anions and a second subunit of PLA2 in the aqueous phase, thereby mimicking PLA2 interaction with an interface (*1*). At this point the initial subunit of the anion-assisted dimer is catalytically competent (E*S) and catalyzes the hydrolysis of PAF, but at a greatly reduced rate. The trapped products in the anion-assisted dimer are the primary nucleation site for protein crystal growth. In this scenario, the subsequent slow hydrolysis of PAF bound in the crystals of the anion-assisted dimer crystal form would yield acetate in one subunit and the tail of the LPC-ether after hydrolysis. Finally, a conformation adjustment of the lyso-headgroup of the LPC-ether product out of the active site of subunit A would yield a structure consistent with that observed in the crystal structure (Figure 1A and 1B).

Regardless of the final source of acetate in the PLA2−acetate complex, we argue the structure is mechanistically informative. Furthermore, this product structure has been obtained in a crystal form that has been suggested to mimic an interface bound form of the enzyme as an anion-assisted dimer (*1*). The anion-assisted dimer crystal form of PLA2 has a requirement of bridging phosphate or sulfate anions and bridging active-site directed ligands in order to attain the dimeric form that mimics PLA2 on an interface. The PLA2−products structure parallels the activated form of the enzyme in several key features. Most notable are the position of the Tyr^{69} loop and the presence of the assisting water w7 observed in the PLA2−products structure. The presence of the w7 assisting water in the acetate product complex further strengthens the oxyanion mechanism outlined in Figure 5 (*10*, *31*). An assisting water mechanism argues that the initial enzyme−substrate complex contains a Ca-coordinated catalytic water (w_c). The catalytic water is bridged to the His^{48} by the assisting water w7. The next step of this mechanism predicts the assisting water w7 bridges His^{48} and the oxygen of the tetrahedral intermediate, which was originally the catalytic water w_c. Previous crystal structures that mimic both a tetrahedral intermediate and the interface bound form of the enzyme have this bridging water w7 (*1*). In contrast, tetrahedral intermediate mimic structures that represent an inactive (*10*) or noninterface bound forms (*26*, *32*) do not contain this bridging water. Here the tetrahedral intermediate oxygen, which was likely derived from the catalytic water, is directly H-bonded to His^{48}. The PLA2−acetate product structure has both an assisting water at the w7 position, and at the same time, an acetate oxygen-His^{48} interaction (Figure 2). It would be interesting to compare this structure to a PLA2−acetate product complex for a crystal form that does not mimic an interface bound form. Curiously, an sn-2 fatty acid product has never been observed in the PLA2 active site despite several crystal forms grown in the presence of fatty acids such as acetate or succinate.

As a mimic of an active monomeric PLA2 at the anionic interface, subunit A of the PLA2−products in the anion-assisted dimer structure with acetate is mechanistically relevant. The interactions of the acetate in the active site are consistent with the product complex proposed in the oxyanion mechanism displayed in Figure 5. As mentioned above, the structure strengthens a model with a Ca-coordinated nucleophilic w_c and an assisting water w7, along with the placement of the 69-loop and interactions of Try^{69} with w7. The location of the acetate also gives a structural perspective about the nature of the rate-limiting step during the breakdown of the tetrahedral intermediate. It should be noted, however, that the structure reported is from a crystal grown at pH 4.6 and may have pH induced structural changes. Previously, the tetrahedral intermediate has been represented by the *sn*-2 phosphates of inhibitors bound in both the anion-assisted PLA2−MJ33 complex (*1*) and the tetrahedral mimic PLA2−MG14 complex (*24*). As shown in Figure 6, the position of the carbonyl carbon in the product acetate can be compared to the *sn*-2 phosphate in competitive inhibitors MJ33 (Figure 6A) and MG14 (Figure 6B) as tetrahedral intermediate mimics. Here acetate's carbonyl carbon lies much closer to both the catalytic calcium and His^{48}. At the same time, the tetrahedral center in MG14 is closer to acetate's carbon center than that of MJ33 in relation to the catalytic dyad. This supports an argument that the bound structure of MG14 (*24*) lies closer to its ultimate position in the fatty acid product than the tetrahedral mimic MJ33. The position of Tyr^{69} is dramatically different when comparing these structures. In the complex with MG14, the sn-3 phosphate group is Ca-coordinated, and Tyr^{69} swings to interact with a nonbridging phosphate oxygen (Figure 6B). In contrast, the acetate and MJ33 complexes (Figure 6A) both have Tyr^{69} interacting with the assisting water w7. The position of the 69-loop and the interactions of Tyr^{69} are clearly an important piece of the mechanistic puzzle. Ideally we would like to establish which PLA2 structure mimics the tetrahedral intermediate most closely. The unfortunate difficulty of tying the present acetate product structural information into the mechanism is that it represents a binary complex, without the bound LPC-ether product in the same active site.

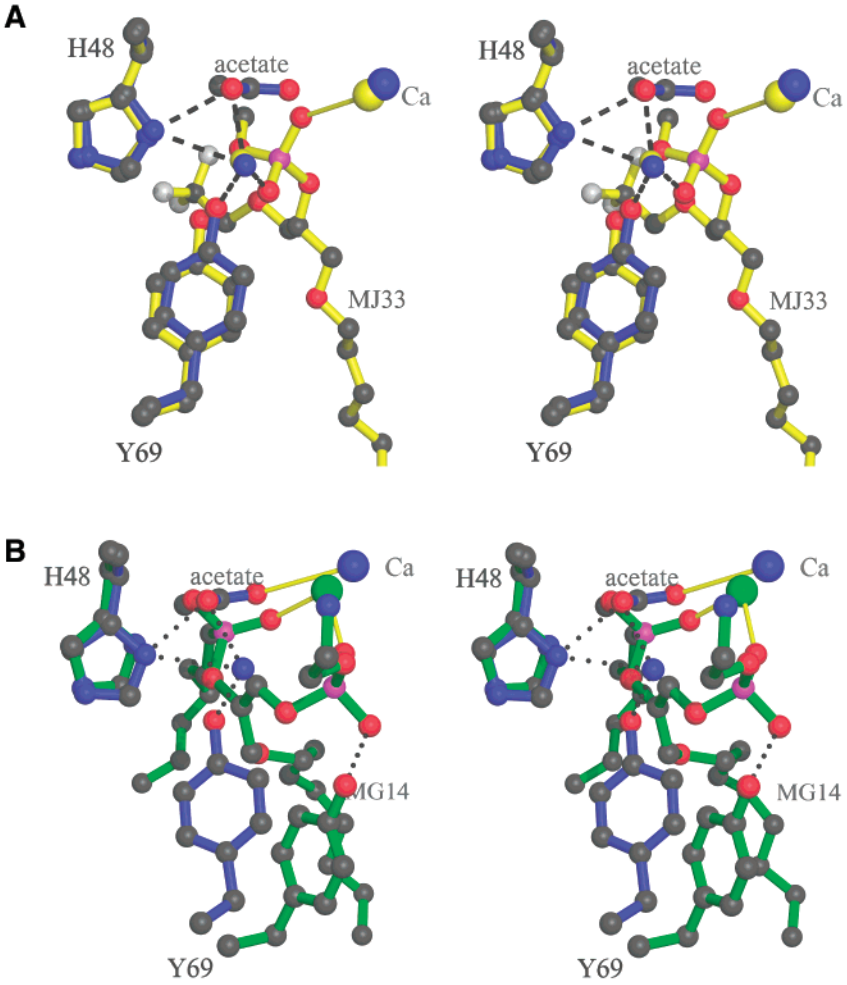

FIGURE 6: (A) Comparison of relative location of the product acetate from subunit A (blue) with the tetrahedral-mimic with porcine PLA2 complexed with MJ33 shown in yellow (*1*). The positions of the active site residues His^{48}, Tyr^{69}, assisting water w7, and the catalytic Ca are likewise shown in blue for the acetate complex structure and yellow for the MJ33 structure. (B) Overlay of the PLA2 structures with bound acetate (blue) and the structure of bovine PLA2 complexed with the tetrahedral mimic MG14 shown in green (*32*). The position of Tyr^{69} shifts from a position of interacting with the calcium-coordinated phosphate group of MG14 to interacting with the assisting water w7 of the acetate bound subunit. The overlay was generated by the alignment of helices 44−55 and 94−107 in PLA2s and rendered using the programs MOLSCRIPT (*33*), POVSCRIPT (http://people.brandeis.edu/~fenn/povscript/), and POVRAY (http://www.povray.org).

APPENDIX

Binding and Protection from Two Ligands. If the two products (L_1 = MA and L_2 = LPC−ether) can bind the catalytic active site singly or together (Scheme 2), the equilibrium probabilities that the catalytic site is bound can be expressed as

$$P_f = 1/Z \text{ for unbound enzyme} \quad (1)$$

$$P_1 = \frac{X_1^*}{K_1^*}\frac{1}{Z} \text{ for } L_1 \text{ bound} \quad (2)$$

$$P_2 = \frac{X_2^*}{K_2^*}\frac{1}{Z} \text{ for } L_2 \text{ bound} \quad (3)$$

$$P_{12} = \frac{X_1^* X_2^*}{K_1^* K_2^{*\#}}\frac{1}{Z} \text{ for both } L_1 \text{ and } L_2 \text{ bound} \quad (4)$$

$$Z = 1 + \frac{X_1^*}{K_1^*} + \frac{X_2^*}{K_2^*} + \frac{X_1^* X_2^*}{K_1^* K_2^{*\#}}$$

is the binding polynomial (5)

Here K_1^* and K_2^* are the dissociation constants for L_1 and L_2, respectively, when each ligand is alone in the catalytic site, and $K_2^{*\#}$ is the dissociation constant for L_2 when L_1 is bound. The corresponding dissociation constant for L_1 when L_2 is bound is defined from the detailed balance condition

$$K_1^{*\#} K_2^* = K_1^* K_2^{*\#} \quad (6)$$

That is, the binding model has three parameters: K_1^*, K_2^*, and the cooperativity factor w:

$$w = K_1^*/K_1^{*\#} = K_2^*/K_2^{*\#} \quad (7)$$

so that $w = 1$ implies independent, $w > 1$ cooperative, and $w < 1$ anticooperative binding. Assume further that the enzyme E* without a ligand in the active site is deactivated by the alkylating agent with rate constant k_0, the E*−L_1 complex with k_1, the E*−L_2 complex with k_2, and the E*−L_1L_2 complex with k_{12}. This gives the relationship for the half-times of inactivation in the absence (t_0) of ligands and in their presence ($t_{1/2}$)

$$\frac{1}{1 - t_0/t_{1/2}} - 1 = \frac{1 + \frac{k_1}{k_0}\frac{X_1^*}{K_1^*} + \frac{k_2}{k_0}\frac{X_2^*}{K_2^*} + \frac{k_{12}}{k_0}\frac{X_1^* X_2^*}{K_1^* K_2^{*\#}}}{\frac{X_1^*}{K_1^*}\left(1 - \frac{k_1}{k_0}\right) + \frac{X_2^*}{K_2^*}\left(1 - \frac{k_2}{k_0}\right) + \frac{X_1^* X_2^*}{K_1^* K_2^{*\#}}\left(1 - \frac{k_{12}}{k_0}\right)} \quad (8)$$

When only ligand L_1 is present in the system, this reduces to

$$\frac{1}{1 - t_0/t_{1/2}} - 1 = \frac{1}{X_1^*} \cdot \frac{K_1^*}{1 - k_1/k_0} + \frac{1}{k_0/k_1 - 1} \quad (9)$$

and analogously for L_2.

When L_1 is LPC-ether, the Scrutton-Utter plot in Figure 4A shows a *y*-intercept that gives $k_1/k_0 = 0.55$ and a slope that gives $K_1^* = 0.06$ mol fraction. Similarly, the plot for myristate alone shows $k_2/k_0 = 0.02$, and the slope gives $K_2^* = 0.10$ mol fraction. Thus, with a *y*-intercept close to zero, myristate affords almost total protection while LPC-ether less than 50%. This suggests that His[48] would be fully protected also if both LPC-ether and myristate were bound to the same catalytic active site ($k_2 \approx k_{12} \approx 0$). When both products are present in equal amounts (X_P^*) in the reaction mixture, this gives

$$\frac{1}{1 - t_0/t_{1/2}} - 1 = \frac{1^*}{X_P^*} \cdot \frac{K_1^* + X_P^* k_1/k_0}{1 - k_1/k_0 + K_1^*/K_2^* + X_P^* w/K_2^*} \quad (10)$$

REFERENCES

1. Pan, Y. H., Epstein, T. M., Jain, M. K., and Bahnson, B. J. (2001) *Biochemistry 40*, 609−17.
2. Epstein, T. M., Yu, B. Z., Pan, Y. H., Tutton, S. P., Maliwal, B. P., Jain, M. K., and Bahnson, B. J. (2001) *Biochemistry 40*, 11411−22.
3. Berg, O. G., Gelb, M. H., Tsai, M. D., and Jain, M. K. (2001) *Chemical Reviews 101*, 2613−2653.
4. Berg, O. G., and Jain, M. K. (2002) *Interfacial Enzyme Kinetics*, Wiley, London.
5. Verheij, H. M., Slotboom, A. J., and de Haas, G. H. (1981) *Rev. Physiol. Biochem. Pharmacol. 91*, 91−203.
6. Yu, B. Z., Poi, M. J., Ramagopal, U. A., Jain, R., Ramakumar, S., Berg, O. G., Tsai, M. D., Sekar, K., and Jain, M. K. (2000) *Biochemistry 39*, 12312−12323.
7. Jain, M. K., Rogers, J., Jahagirdar, D. V., Marecek, J. F., and Ramirez, F. (1986) *Biochim. Biophys. Acta 860*, 435−47.
8. Berg, O. G., Yu, B. Z., Rogers, J., and Jain, M. K. (1991) *Biochemistry 30*, 7283−97.
9. Ramirez, F., and Jain, M. K. (1991) *Proteins: Struct. Funct. Genet. 9*, 229−39.
10. Epstein, T. M., Yu, B.-Z., Pan, Y. H., Tutton, S. P., Maliwal, B. P., Jain, M. K., and Bahnson, B. J. (2001) *Biochemistry 40*, 11411−11422.
11. Jain, M. K., and Rogers, J. (1989) *Biochim Biophys Acta 1003*, 91−7.
12. Rogers, J., Yu, B. Z., Serves, S. V., Tsivgoulis, G. M., Sotiropoulos, D. N., Ioannou, P. V., and Jain, M. K. (1996) *Biochemistry 35*, 9375−84.
13. Otwinowski, Z., and Minor, W. (1997) *Methods Enzymol. 276*, 307−326.
14. Navaza, J. (2001) *Acta Crystallogr., Sect. D: Biol Crystallogr. 57*, 1367−72.
15. CCP4. (1994) *Acta Crystallogr., Sect. D 50*, 760−763.
16. Yeates, T. O. (1997) *Methods Enzymol. 276*, 344−358.
17. Brunger, A. T., Adams, P. D., Clore, G. M., Delano, W. L., Gros, P., Grosse-Kunstleve, R. W., Jiang, J.-S., Kuszewski, J., Nilges, N., Pannu, N. S., Read, R. J., Rice, L. M., Simonson, T., and Warren, G. L. (1998) *Acta Crystallogr., Sect. D 54*, 905−921.
18. Sack, J. S., and Quiocho, F. A. (1997) *Methods Enzymol. 277*, 158−173.
19. Jones, T. A., Zou, J. Y., Cowan, S. W., and Kjeldgaard, M. (1991) *Acta Crystallogr., Sect. A 47*, 110−119.
20. Jain, M. K., and Maliwal, B. P. (1993) *Biochemistry 32*, 11838−46.
21. Jain, M. K., Yu, B. Z., Rogers, J., Ranadive, G. N., and Berg, O. G. (1991) *Biochemistry 30*, 7306−17.
22. Yu, B. Z., Berg, O. G., and Jain, M. K. (1993) *Biochemistry 32*, 6485−92.
23. Dijkstra, B. W., Kalk, K. H., Hol, W. G., and Drenth, J. (1981) *J. Mol. Biol. 147*, 97−123.
24. Scott, D. L., Otwinowski, Z., Gelb, M. H., and Sigler, P. B. (1990) *Science 250*, 1563−6.
25. Steiner, R. A., Rozeboom, H. J., de Vries, A., Kalk, K. H., Murshudov, G. N., Wilson, K. S., and Dijkstra, B. W. (2001) *Acta Crystallogr., Sect. D: Biol. Crystallogr. 57*, 516−526.
26. Sekar, K., Eswaramoorthy, S., Jain, M. K., and Sundaralingam, M. (1997) *Biochemistry 36*, 14186−91.
27. Dupureur, C. M., Yu, B. Z., Jain, M. K., Noel, J. P., Deng, T., Li, Y., Byeon, I. J., and Tsai, M. D. (1992) *Biochemistry 31*, 6402−13.
28. Jain, M. K., Yu, B. Z., and Berg, O. G. (1993) *Biochemistry 32*, 11319−29.
29. Jain, M. K., and de Haas, G. H. (1981) *Biochim. Biophys. Acta 642*, 203−11.
30. Jain, M. K., van Echteld, C. J., Ramirez, F., de Gier, J., de Haas, G. H., and van Deenen, L. L. (1980) *Nature 284*, 486−7.
31. Yu, B. Z., Rogers, J., Nicol, G. R., Theopold, K. H., Seshadri, K., Vishweshwara, S., and Jain, M. K. (1998) *Biochemistry 37*, 12576−87.
32. Sekar, K., Kumar, A., Liu, X., Tsai, M. D., Gelb, M. H., and Sundaralingam, M. (1998) *Acta Crystallogr., Sect. D: Biol. Crystallogr. 54*, 334−41.
33. Kraulis, P. J. (1991) *J. Appl. Crystallogr. 24*, 946−950.

BI026922R